Journal of
Applied Remote Sensing

Bidirectional reflectance effects over flat land surface from the charge-coupled device data sets of the HJ-1A and HJ-1B satellites

Feng Zhao
Xingfa Gu
Tao Yu
Wout Verhoef
Yiqing Guo
Yongming Du
Hong Shang
Huijie Zhao

SPIE

Bidirectional reflectance effects over flat land surface from the charge-coupled device data sets of the HJ-1A and HJ-1B satellites

Feng Zhao,[a] Xingfa Gu,[b] Tao Yu,[b] Wout Verhoef,[c] Yiqing Guo,[a] Yongming Du,[b] Hong Shang,[a] and Huijie Zhao[a]

[a]Beijing University of Aeronautics and Astronautics, Key Laboratory of Precision Opto-Mechatronics Technology, Ministry of Education, School of Instrument Science and Opto-Electronics Engineering, No. 37 Xueyuan Road, Beijing 100191, China
zhaofeng@buaa.edu.cn

[b]Chinese Academy of Sciences, Institute of Remote Sensing and Digital Earth, No. 20 Datun Road, Beijing 100101, China

[c]University of Twente, Faculty of Geo-Information Science and Earth Observation (ITC), Hengelosestraat 99, P.O. Box 6, 7500 AA Enschede, The Netherlands

Abstract. The HJ-1A and HJ-1B satellites were launched successfully on September 6, 2008. For effective monitoring of the environmental and natural disasters, both HJ-1A and HJ-1B carry a charge-coupled device (CCD) sensor, with each CCD sensor containing two cameras, which results in a ground swath of about 700 km for each satellite. The CCD can make cross-track multiple view angle measurements with a field of view of >40 deg. The Earth's surface can be covered completely within 48 h in four spectral bands from 0.43 to 0.90 μm. We have presented a method of extracting the hemispherical-directional reflectance factor (HDRF) from CCD imagery and normalizing HDRF to a standard geometric situation. After geometric correction and registration, radiometric calibration, and correction for atmospheric effects, multitemporal HDRFs were obtained for the flat land surface located in Northern China with different land cover types. The angular observations were extracted from a series of overpasses of the CCD aboard HJ-1A and HJ-1B. We then inverted the HDRFs by the semiempirical kernel-driven bidirectional reflectance distribution function (BRDF) model and normalized the HDRFs to nadir-viewing direction. This study shows the significance of directional effects in the HJ-1A and HJ-1B CCD data and the feasibility of normalizing HDRFs' CCD data when the angular effects must be taken into account. [DOI: 10.1117/1.JRS.7.073466]

Keywords: HJ-1A satellite; HJ-1B satellite; charge-coupled device (CCD); hemispherical-directional reflectance factor; bidirectional reflectance distribution function; normalize.

Paper 13235 received Jul. 4, 2013; revised manuscript received Oct. 11, 2013; accepted for publication Nov. 8, 2013; published online Dec. 16, 2013.

1 Introduction

Researchers have indicated that the number and strength of extreme climate events and natural disaster events, such as storms, hurricanes, typhoons, floods, droughts, and tornadoes, have increased significantly over the past 10 to 20 years, and situations are expected to become more severe in the coming years.[1] Chinese citizens face even more environmental challenges with the country's rapid economic growth. For timely and effective monitoring of the environmental and natural disasters, a small satellite constellation (HJ-1), which is composed of two optical satellites (HJ-1A and HJ-1B) and one synthetic aperture radar (SAR) satellite (HJ-1C), was proposed. The HJ-1A and HJ-1B satellites were launched successfully on September 6, 2008.[2]

Each satellite carries a charge-coupled device (CCD) sensor which contains two identical cameras (CCD1 and CCD2). Detailed technical specifications of the cameras can be found

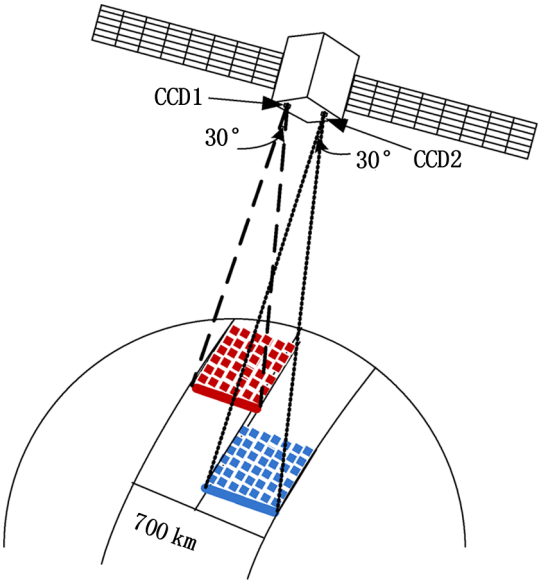

Fig. 1 Schematic sketch of the HJ-1A and HJ-1B payloads.

in Ref. 3. The CCD sensor has a pushbroom scanning mechanism similar to a high-resolution visible sensor (HRV) on the Satellite Pour l'Observation de la Terre (SPOT) platform. In order to provide imaging data over large areas, CCD1 and CCD2 offer an oblique viewing capability, with the view angle tilting ± 15 deg relative to the vertical, as shown in Fig. 1. The field of view (FOV) of CCD1 and CCD2 is relatively large, about 30 deg. As a result, the nominal variation of the view zenith angle for a given point on the Earth's surface per overpass is from -30 to $+30$ deg, where a minus sign indicates view angles in the forward scatter direction and a plus sign indicates view angles in the backscatter direction. Taking into account the effect of the Earth's surface curvature, view zenith angles of up to $+47$ deg from the nadir have been sampled in this study. Observations from a single orbit were acquired at different viewing geometries relative to the source of illumination (the sun); some measurements were taken in the forward direction and some in the backward direction. For one optical satellite, the revisit cycle of the multispectrum CCD camera is 96 h. Because the HJ-1A and HJ-1B satellites are in the same orbit with a phase difference of 180 deg, the repeat cycle of the CCD sensor is reduced to <48 h. Therefore, the HJ-1A and HJ-1B satellite sensors have the capability of sampling the hemispherical-directional reflectance factor (HDRF) over a wide range of view zenith angle in a short time period in four spectral bands from 0.43 to 0.90 μm, which makes them attractive for detecting land cover changes, vegetation dynamics monitoring, and primary production estimates.

The variations of the sun–target–sensor geometry can cause large fluctuations in the time series of data acquired by the CCDs of HJ-1A and HJ-1B. The fluctuations may originate either from the changes in the atmospheric path or from the non-Lambertian behavior of a surface target.[4] Roujean et al.[5] demonstrated that the short-term variations in NOAA/AVHRR multitemporal data sets were essentially due to the surface bidirectional effects, while the atmospheric directional effects and other sources of fluctuation remain of lower amplitude. Surface directional reflectance effects have been observed experimentally by means of ground measurements by a number of researchers,[6–12] establishing as a fact that most surfaces have a reflectance behavior far from Lambertian. Recent radiation transfer model intercomparison (RAMI) exercises in this area have shown the close relationship between the three-dimensional (3-D) geometry of natural surfaces and their angular reflectance properties.[13,14]

This non-Lambertian behavior of surface targets can significantly alter the observed reflected radiance under different view directions and, thereby, can affect the detection of target temporal evolutions. Leroy and Roujean,[4] Roujean et al.,[5] and Ba et al.[15] demonstrated the evident existence of surface directional reflectance effects in NOAA/AVHRR multitemporal data sets. For the

moderate resolution imaging spectrometer (MODIS), images from multiple days were collected, and surface directional reflectance factors were retrieved to derive operationally the bidirectional reflectance distribution function (BRDF) and albedo product.[16]

To our knowledge, no pertinent research has been reported to investigate the BRDF effects using data sets acquired by HJ-1A and HJ-1B CCDs. The purpose of this study is to assess the magnitude of directional effects over flat land surface from the CCD data sets of HJ-1A and HJ-1B. In addition, if this magnitude is significant, our goal is to attempt to normalize HDRF to a standard sun–target–sensor geometry defined by the user. First, the preprocessing procedures of compositing the multitemporal BRDF data sets of the research area were briefly introduced. Then the semiempirical kernel-driven BRDF model and its inversion were presented. The performance of the model inversion was tested with the field experimental reflectance data. Finally, the anisotropy was analyzed with four images acquired by HJ-1A and HJ-1B CCDs over a flat rural region located in Northern China. The performance of the kernel-driven model inversion for these data sets was evaluated. The paper was closed with a brief conclusion and discussion of this study.

2 Data Sets and Methods

2.1 *Study Area and Retrieval of Hemispherical-Directional Reflectance Factors*

The area selected for this study lies in the southern part of Hebei Province, as shown in Fig. 2. The area is relatively flat and in a rural region, away from the urban areas. The land is planted mainly in wheat and corn. The selected images were obtained by the HJ-1A and HJ-1B CCDs during the period from July 2, 2009 to July 12, 2009. The time period coincided with the growing stage for corn and was kept short to ensure that the changes in the vegetation cover were small.

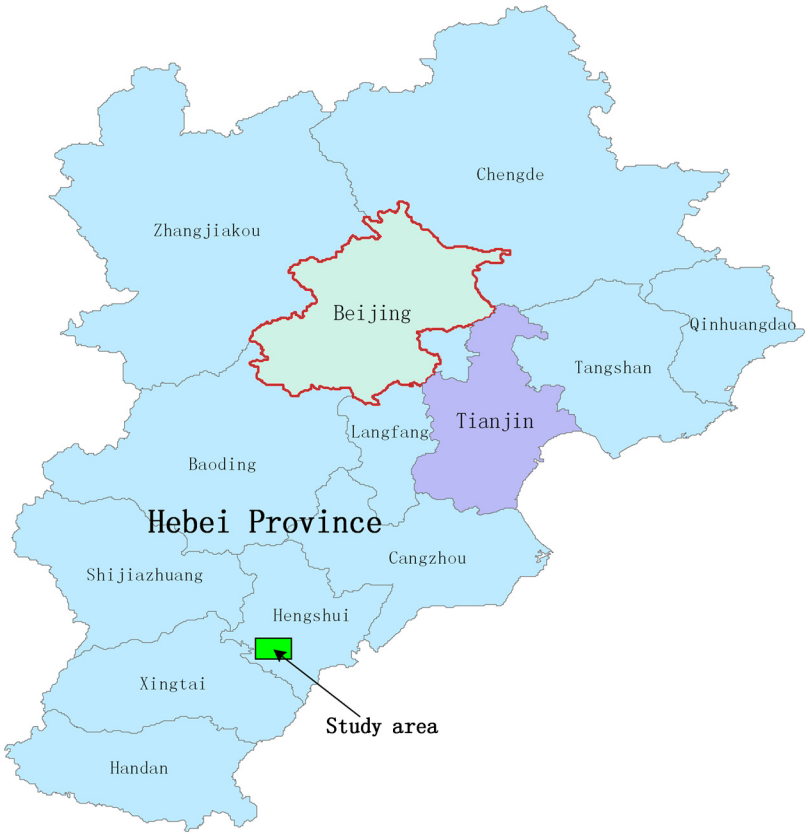

Fig. 2 Location of the study area.

The next step consisted of screening the cloudy images of the study area. The images would be rejected whenever they appeared cloudy by visual inspection or when the presence of clouds made it impossible to determine the exact location of the study area.

In total, four images were selected with a variety of scan angles, including forward and backward view angles (−47 to +47 deg). The collected images are level-2 products from the China Center for Resource Satellites. The solar/view zenith and azimuth angles of the images were then computed based on the metadata.

The calibration coefficients of the CCD's four spectral bands are supplied together with the level-2 data to convert the digital number to radiance. Atmospheric corrections were then applied to the radiance images by using the Fast Line-of-sight Atmospheric Analysis of Spectral Hypercubes (FLAASH) module in the ENVI 4.7 software. The atmospheric correction for all images was based on a mid-latitude summer atmospheric model and rural aerosol model. The input values of the scene and sensor information, such as sensor altitude and flight date and time, were provided by the metadata. The default values were given to other unknown inputs like visibility (40 km), aerosol scale height (2 km), and carbon dioxide mixing ratio (390 ppm), as defined in the FLAASH. The FLAASH module was then executed to compute ground surface reflectance factors under the guidelines given in the FLAASH User's Guide.[17]

After the computations of solar/view angles and reflectance factors of all 4 days' data, the common regions in them were retrieved by using the layer stacking tool in the ENVI software. Because of the large FOV and high temporal resolution of HJ-1A and HJ-1B CCDs, a large common area was retrieved after the image compositing.

2.2 *Kernel-Driven Model and its Inversion*

The final step was to apply the semiempirical kernel-driven BRDF model to invert the multiple-temporal atmospherically corrected directional reflectance factors to normalize them to user-defined sun–target–sensor geometry. In this paper, we used the linear kernel-driven model proposed by Wanner et al.,[18] which has been validated[19,20] and applied for MODIS land surface BRDF/albedo product.[16] In this model, the BRDF is expanded into a linear sum of terms (the so-called kernels), characterizing different scattering modes. This can be generally described using the following expression:

$$R(\theta_s, \theta_v, \varphi) = f_{\text{iso}} + f_{\text{vol}} k_{\text{vol}}(\theta_s, \theta_v, \varphi) + f_{\text{geo}} k_{\text{geo}}(\theta_s, \theta_v, \varphi), \tag{1}$$

where k_{vol} and k_{geo} are the kernels (i.e., known functions of illumination and viewing geometry) which describe volume and geometric scatterings from the target, respectively, θ_s is the solar zenith angle, θ_v is the view zenith angle, φ is the relative azimuth of the solar and view directions, f_{vol} and f_{geo} are the weights for volumetric and geometric kernels, respectively, and f_{iso} is a constant corresponding to isotropic reflectance. In this study, the RossThick–LiTransit kernels combination was used as the BRDF model. This combination may give better results than the model currently used in the operational MODIS BRDF/albedo algorithm.[21] The expressions of the kernels can be found in Ref. 21 and are not shown here.

To invert the kernel-driven model with m observations of HDRF (noted as $y_{\text{obs}}(1)$, $y_{\text{obs}}(2), \ldots, y_{\text{obs}}(m)$), we used the following equation:

$$y_{\text{obs}}(i) = A[i,3] \times X[3] + \varepsilon_i, (i = 1, 2, \ldots, m), \tag{2}$$

where $A[i,3] = [\,1 \;\; k_{\text{geo}}(i) \;\; k_{\text{vol}}(i)\,]$ is determined solely by the sun–target–sensor geometry, $X[3] = [\,f_{\text{iso}} \;\; f_{\text{geo}} \;\; f_{\text{vol}}\,]$ is the parameter vector to be inverted, and ε_i is the error term. Writing them in the matrix notation, we have the following:

$$Y_{\text{obs}}[m] = \begin{bmatrix} y_{\text{obs}}(1) \\ y_{\text{obs}}(2) \\ \vdots \\ y_{\text{obs}}(m) \end{bmatrix} \quad \text{and} \quad A[m,3] = \begin{bmatrix} 1 & k_{\text{geo}}(1) & k_{\text{vol}}(1) \\ 1 & k_{\text{geo}}(2) & k_{\text{vol}}(2) \\ \vdots & \vdots & \vdots \\ 1 & k_{\text{geo}}(m) & k_{\text{vol}}(m) \end{bmatrix}.$$

Finally, the solution of the kernel parameters can be written as

$$X[3] = \begin{bmatrix} f_{\text{iso}} \\ f_{\text{geo}} \\ f_{\text{vol}} \end{bmatrix} = (A[m,3]\prime \times A[m,3])^{-1} \times A[m,3]\prime \times Y_{\text{obs}}[m]. \tag{3}$$

With more than three uncorrelated multiangular observations, Eq. (3) can provide estimates of the three parameters. Using Eq. (1) in forward mode and the inverted parameters, the reflectance factor under the standard sun–target–sensor can be estimated.

3 Results and Discussion

First, the validation results of the linear semiempirical BRDF model with *in situ* HDRF measurements are given. Next, the distributions of HDRFs for HJ-1A and HJ-1B CCD data are analyzed and inverted.

3.1 *Validation of the Linear Semiempirical BRDF Model*

The semiempirical model approach will be useful only if the models can be shown to be adequate, which demands that it be tested first. Surface HDRFs obtained *in situ* is essential if we want to evaluate the models in isolation from the other confounding influences (e.g., the effects of the atmosphere) and in a relatively controlled manner. The data were acquired in 2004 at the China National Experimental Station for Precision Agriculture in Xiaotangshan County, which is located in Changping District, Beijing, China. The experimental site consisted mainly of winter wheat. An Analytical Spectral Devices FieldSpec Pro spectrometer (Analytical Spectral Devices, Boulder, Colorado) mounted on a goniometric instrument was used to measure the wheat canopy multiangular radiation. Multiangular measurements were carried out with viewing zenith angles from −60 deg (forward direction) to +60 deg (backward direction) at 10-deg intervals in the principal plane (PP, where the sun, the target, and the sensor are aligned in the same plane). Zhao et al.[22] gave detailed information about this experiment.

In this study, HDRFs in two characteristic spectral bands of vegetation were used to invert the kernel-driven model: red (666 nm) and NIR (850 nm), with the solar zenith and azimuth angles being 36.3 and 177 deg, respectively. To test the performance of the model and its

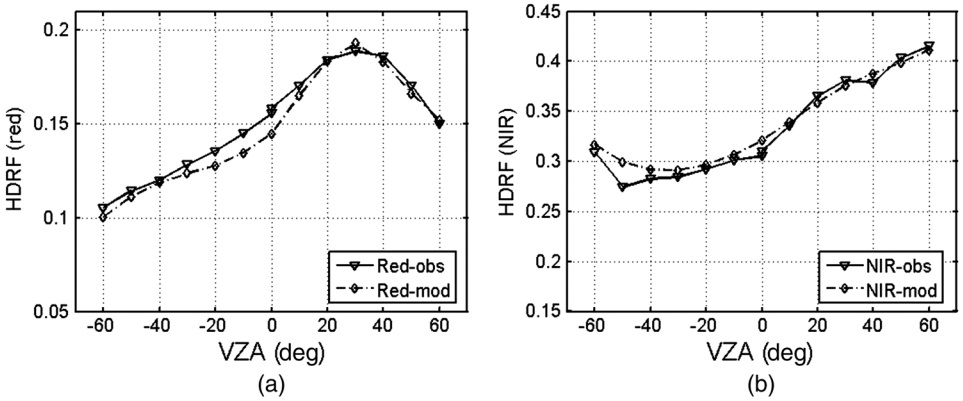

Fig. 3 Observed versus modeled HDRF distributions in PP for the red (a) and NIR (b) bands.

inversion, we reconstructed the HDRFs by using Eq. (2) and the inverted parameters. Figure 3 shows the comparisons of observed and modeled (or reconstructed) HDRF profiles in PP. The root-mean-square error (RMSE) between observed and modeled HDRFs is 0.006 for the red band and 0.01 for the NIR band. For the measured HDRFs in the red band in Fig. 3(a), a local maximum value appears around the antisolar direction, called the hotspot effect. Modeled (or reconstructed) profiles of HDRFs adequately replicate this phenomenon. Overall, the model fits are considered very satisfactory, bearing in mind the likely sources of error in the measured reflectance factors and the approximations made in the model derivation.

3.2 *Directional Effects of HJ-1A's and HJ-1B's CCD Data*

As stated before, our study area lies in a flat and rural region, with relatively monotonous land cover types. After screening the cloud contaminated images between July 2, 2009 and July 12, 2009, we chose the image data from the following 4 days: July 2, July 3, July 9, and July 12. The preprocessed data for the blue band (band 1 in each sensor, 0.43 to 0.52 μm) are shown in Fig. 4. The values of these HDRFs are in the range [0.0309, 0.2122].

Next, Eq. (4) was used to invert the BRDF data sets. Equation (2) was used to normalize these BRDF values to the nadir view geometry with the solar zenith angle and the relative difference between solar and view azimuth angles being 20 and 0 deg, respectively. The normalized HDRFs and inverted model parameters are shown in Fig. 5. The normalized HDRFs [Fig. 5(a)] are still in the range [0.0309, 0.2122], ruling out the apparent failure of the BRDF model inversion. The distribution of isotropic model parameters [f_{iso}, Fig. 5(b)] shows a similar pattern with the normalized HDRFs [Fig. 5(a)], consistent with the physical meaning that it

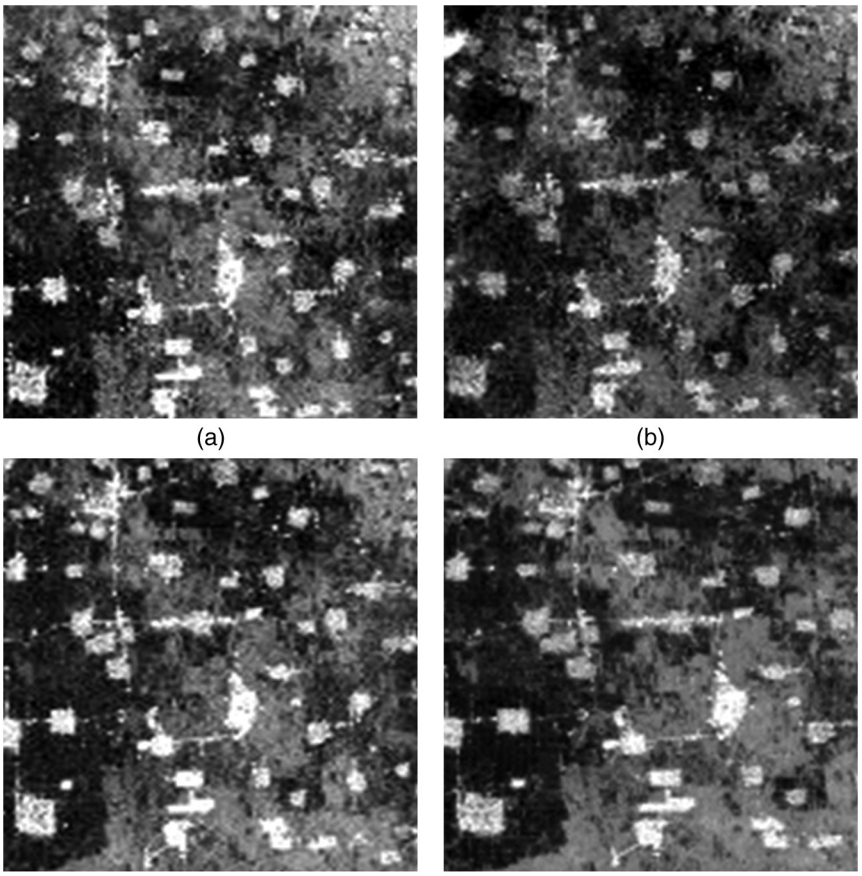

Fig. 4 Images in the blue band of CCD for (a) 7/2, (b) 7/3, (c) 7/9, and (d) 7/12, 2009.

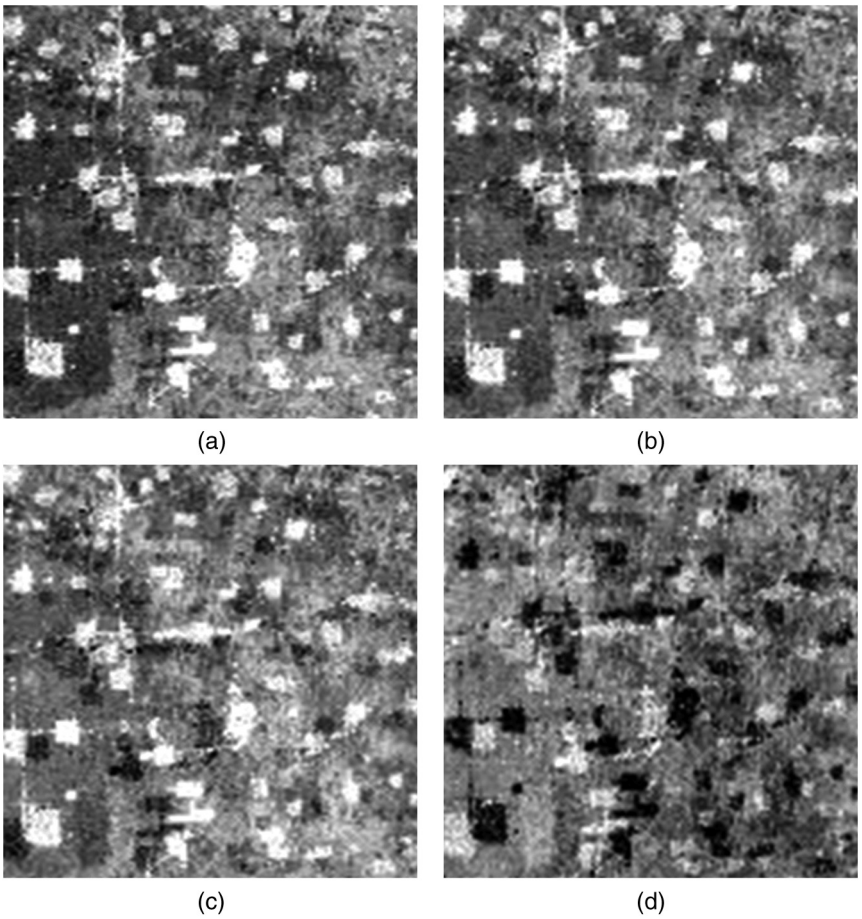

Fig. 5 Normalized results and model parameters for HDRFs in Fig. 4, using the kernel-driven BRDF model: (a) normalized reflectance factor, (b) isotropic model parameters, f_{iso}, (c) geometric model parameters, f_{geo}, and (d) volumetric model parameters, f_{vol}.

represents the reflectance factor observed at nadir with the sun at zenith. However, due to the approximate nature of the kernels, determining what information is contained within the parameters f_{vol} and f_{geo} is not straightforward. The problem lies in the fact that the volumetric and geometric kernels are not necessarily orthogonal because volumetric and geometric effects are not mutually exclusive.[23]

To further analyze the anisotropy observed by the HJ-1A and HJ-1B CCDs and to evaluate the performance of the kernel-driven model inversion, three land cover types were selected: corn in the elongation stage (type 1), fallow farmland after the harvest of the winter wheat (type 2), and a village of farmers (type 3). The cover types were determined according to the false color composite map [R4G3B2, Fig. 6(a)] and historical land-use maps. The average values of 5×5 pixels' HDRFs in the blue band were used here to analyze their distribution with the view zenith angles. These values were then used to invert the kernel-driven BRDF model [Eq. (2)] so as to reconstruct the profiles under the same sun–target–sensor geometry.

All three types of targets show distinct anisotropic reflectance distributions with the view zenith angles, and the HDRFs in the backward directions generally are larger than those in the forward directions. For type 3 [Fig. 6(d)], which has evident 3-D structures of buildings, a clear hotspot phenomenon appears around the backscattering direction. Therefore, the directional effects in the HJ-1A and HJ-1B CCD data cannot be ignored. Similar non-Lambertian features exist in the other three bands.

By inverting the kernel-driven BRDF model and reconstructing the profiles for these three types [Figs. 6(b)–6(d)], we plotted the observed and modeled HDRFs together to evaluate the

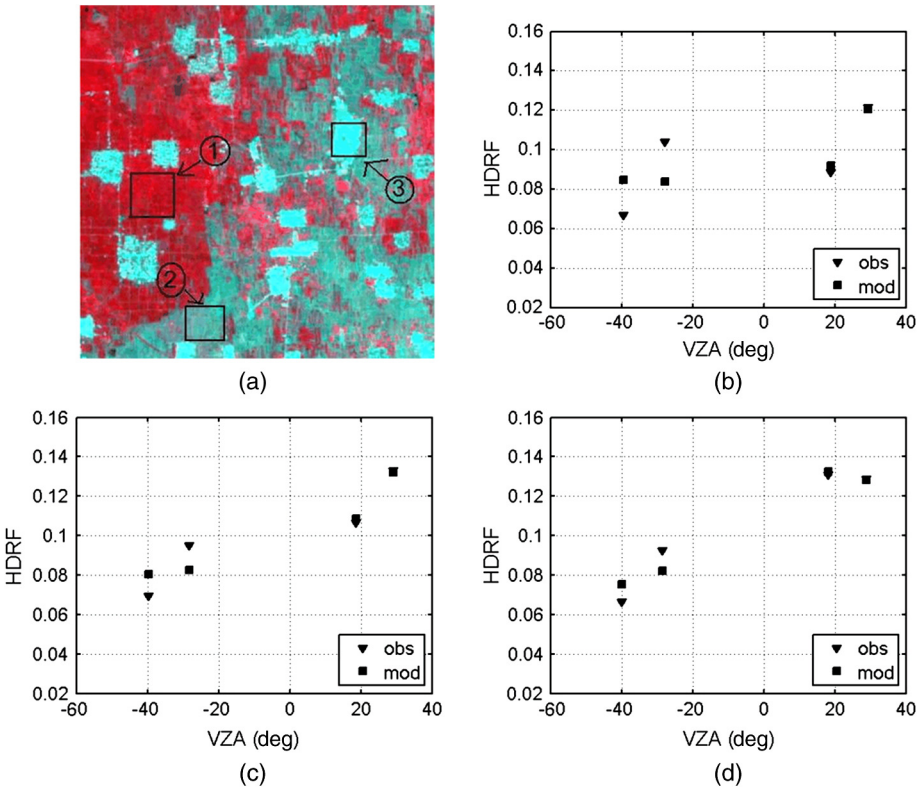

Fig. 6 Observed versus modeled HDRF distributions in the blue band for three different land cover types: (a) false color composite of part of the study area, black rectangle shows three land cover types. Observed versus modeled HDRF distributions for type 1 (b), type 2 (c), and type 3 (d).

inversion. The reconstructed HDRFs generally follow the patterns of the observed ones, although with some bias, especially for type 1 [Fig. 6(b)]. The RMSEs for types 1, 2, and 3 are 0.0136, 0.008, and 0.007, respectively.

4 Conclusions

The purpose of this study was to assess the magnitude of BRDF effects in HJ-1A and HJ-1B CCDs' data over flat land surfaces, their dependence on land cover, and the possibility of correcting for these effects as part of the compositing process. The study area lies in Northern China and we used cloud-free CCD images over 10 days during the green period in 2009. All images were atmospherically corrected, coregistered, and resampled. Uniform sample sites representing dense and fallow cropland and buildings were chosen. The results showed that the typical BRDF effects exist in the HJ-1A and HJ-1B CCD data. Therefore, directional effects should be considered when comparing multitemporal CCD data under different view directions. Our study demonstrated the feasibility of inversion of the kernel-driven BRDF model to normalize HDRFs to the standard sun–target–sensor geometry after retrieving HDRFs from the multiday CCD data.

Even though the observed HDRFs and the reconstructed HDRFs generally show close agreement, bias still exists, which may be induced by the uncertainties of preprocessing data. For the atmospheric correction, while molecular scattering and ozone absorption effects may be corrected relatively easily with the climatologic data, water vapor and aerosol amounts are highly variable in space and time and, consequently, introduce errors. In addition, errors in the process of coregistering and resampling the multidays CCD data and the difference of spatial resolutions under different viewing angles can result in disagreements.

Much work remains to be completed to validate and evaluate the results in this study. The accuracy of retrieved HDRFs and inverted model parameters should be assessed carefully with the field and airborne experiments on the selected sites. The performance of the kernel-driven BRDF model should also be tested with more measured data, especially under limited sampling capabilities, such as HJ-1A and HJ-1B CCDs.

Acknowledgments

This work is supported by the Chinese Defense Advanced Research Program of Science and Technology, China (Grant No. 07K00100KJ), the Chinese Natural Science Foundation under Project 41371325 and 40901156, the Civil Aerospace Technology Pre-research Project of China (Grant No. D040201-03), and the State Key Laboratory of Remote Sensing Science (Grant No. 2009kfjj022). The authors would like to thank the CRESDA Web site hosted by CASC, China, for providing the HJ-1A and HJ-1B CCD data. Thanks also go to Dr. Zhang Hao, Qin Ji, and Zhi Jingkuo for helpful discussions and preprocessing the data.

References

1. S. G. Philander, *Encyclopedia of Climate Change and Global Warming*, SAGE Publications, California (2008).
2. Q. Wang, C. Wu, and Q. Li, "Environment satellite 1 and its application in environment monitoring," *J. Remote Sens.* **14**(1), 104–121 (2010).
3. China Center for Resources Satellite Data and Application, http://www.cresda.com/n16/n1130/n1582/8384.html (19 November 2013).
4. M. Leroy and J. L. Roujean, "Sun and view angle corrections on reflectances derived from NOAA/AVHRR data," *IEEE Trans. Geosci. Remote Sens.* **32**(3), 684–697 (1994), http://dx.doi.org/10.1109/36.297985.
5. J. L. Roujean et al., "Evidence of surface reflectance bidirectional effects from a NOAA/AVHRR multi-temporal data set," *Int. J. Remote Sens.* **13**(4), 685–698 (1992), http://dx.doi.org/10.1080/01431169208904146.
6. D. S. Kimes, "Dynamics of directional reflectance factor distributions for vegetation canopies," *Appl. Opt.* **22**(9), 1364–1372 (1983), http://dx.doi.org/10.1364/AO.22.001364.
7. D. S. Kimes et al., "Directional reflectance factor distributions of a cotton row crop," *Int. J. Remote Sens.* **5**(2), 263–277 (1984), http://dx.doi.org/10.1080/01431168408948807.
8. D. S. Kimes et al., "Optimal directional view angles for remote sensing missions," *Int. J. Remote Sens.* **5**(6), 887–908 (1984), http://dx.doi.org/10.1080/01431168408948876.
9. D. S. Kimes et al., "Directional reflectance factor distributions for cover types of Northern Africa," *Remote Sens. Environ.* **18**(1), 1–19 (1985), http://dx.doi.org/10.1016/0034-4257(85)90034-3.
10. H. Chen et al., "Predicting leaf area index in wheat using an improved empirical model," *J. Appl. Remote Sens.* **7**(1), 073577 (2013), http://dx.doi.org/10.1117/1.JRS.7.073577.
11. J. A. Naupari, L. A. Vierling, and J. U. H. Eitel, "Delineating native and invasive plant functional groups in shrub-steppe vegetation using bidirectional reflectance," *J. Appl. Remote Sens.* **7**(1), 073563 (2013), http://dx.doi.org/10.1117/1.JRS.7.073563.
12. J. S. Czapla-Myers, K. J. Thome, and S. F. Biggar, "Calibration and characterization of a digital camera for bidirectional reflectance distribution function retrieval of vicarious calibration sites," *J. Appl. Remote Sens.* **3**(1), 033519 (2009), http://dx.doi.org/10.1117/1.3116662.
13. B. Pinty et al., "The radiation transfer model intercomparison (RAMI) exercise," *J. Geophys. Res.* **106**(D11), 11937–11956 (2001), http://dx.doi.org/10.1029/2000JD900493.
14. J. L. Widlowski et al., "The fourth radiation transfer model intercomparison (RAMI-IV): proficiency testing of canopy reflectance models with ISO-13528," *J. Geophys. Res.: Atmos.* **118**(13), 1–22 (2013), http://dx.doi.org/10.1002/jgrd.50497.
15. M. B. Ba et al., "Reduction of bidirectional effects in NOAA-AVHRR data acquired during the HAPEX-Sahel experiment," *J. Hydrol.* **188–189**, 725–748 (1997), http://dx.doi.org/10.1016/S0022-1694(96)03168-X.

16. A. H. Strahler et al., "MODIS BRDF/albedo product: algorithm theoretical basis document, NASA EOS-MODIS Document," Version 5.0, MODIS documentation (1999).
17. VIS, ITT, *Atmospheric Correction Module: QUAC and FLAASH User's Guide*, August 2009 Edition., Module Version 4 (2009).
18. W. Wanner, X. Li, and A. H. Strahler, "On the derivation of kernels for kernel-driven models of bidirectional reflectance," *J. Geophys. Res.: Atmos.* **100**(D10), 21077–21089 (1995), http://dx.doi.org/10.1029/95JD02371.
19. B. Hu et al., "Validation of kernel-driven semiempirical models for the surface bidirectional reflectance distribution function of land surfaces," *Remote Sens. Environ.* **62**(3), 201–214 (1997), http://dx.doi.org/10.1016/S0034-4257(97)00082-5.
20. X. Huang et al., "Analysis of BRDF and albedo retrieved by kernel-driven models using field measurements," *IEEE J. Sel. Top. Appl. Earth Obs. Remote Sens.* **6**(1), 149–161 (2013), http://dx.doi.org/10.1109/JSTARS.2012.2208264.
21. F. Gao et al., "Comparison and validation of the new Li-Transit kernel," *Remote Sens. Rev.* **19**(1–4), 205–224 (2000), http://dx.doi.org/10.1080/02757250009532419.
22. F. Zhao et al., "A spectral directional reflectance model of row crops," *Remote Sens. Environ.* **114**(2), 265–285 (2010), http://dx.doi.org/10.1016/j.rse.2009.09.018.
23. F. Gao et al., "Detecting vegetation structure using a kernel-based BRDF model," *Remote Sens. Environ.* **86**(2), 198–205 (2003), http://dx.doi.org/10.1016/S0034-4257(03)00100-7.

Feng Zhao is a lecturer at the Beijing University of Aeronautics and Astronautics. He received his PhD in remote sensing from the Institute of Remote Sensing Applications (IRSA), CAS, in 2008. He is the author of more than 15 journal papers. His current research interests include radiation transfer in vegetation and atmosphere and quantitative remote sensing modeling and applications.

Xingfa Gu is a professor at the Institute of Remote Sensing and Digital Earth, CAS. He received his PhD in physical remote sensing from Paris Diderot University (Paris 7) in 1991. He is the author of more than 200 papers, of which 40 papers were indexed by SCI and 68 papers were indexed by EI. His current research interests include calibration of satellite payloads, quantitative study of ground surface, evaluation of new payloads, observation of aerosol and atmospheric correction, and processing and application of remote-sensing data.

Biographies and photographs of the other authors are not available.